# Supporting Information

## Copper-Barium-Decorated-Carbon-Nanotube Nanocomposite for Electrocatalytic $CO_2$ Reduction to C2 Products

*Feng-Yi Wu,[1] Hsin-Jung Tsai,[1] Tsung-Ju Lee,[1] Zih-Yi Lin,[1] Kang-Shun Peng,[1] Pei-Hsuan Chen,[1] Nozomu Hiraoka,[2] Yen-Fa Liao,[2] Chih-Wei Hu,[2] Shao-Hui Hsu,[3] Ying-Rui Lu,[2,*] Sung-Fu Hung,[1,*]*

*[1]Department of Applied Chemistry, National Yang Ming Chiao Tung University, Hsinchu 300, Taiwan.*

*[2]National Synchrotron Radiation Research Center, Hsinchu 300, Taiwan*

*[3]Taiwan Semiconductor Research Institute, National Applied Research Laboratories, Hsinchu 300, Taiwan.*

Email: sungfuhung@nycu.edu.tw

**This file includes:**

Experimental Section

Supplementary Figures 1 to 18

Supplementary Table 1

**Experimental Section**

***Chemicals****:* $Cu(NO_3)_2{\cdot}3H_2O$ (99%) and $Ba(NO_3)_2{\cdot}$(99%) were purchased from ACROS. $K_2CO_3$ (99%) was purchased from Alfa-Aesar. Multi-walled carbon nanotube (OD = 10-20 nm, L = 1-2 μm, > 95%) was purchased from Biotech. $H_2SO_4$ (96%) and $HNO_{3(aq)}$ (70%) were purchased from AENCORE. Nafion solution (5% in lower aliphatic alcohols and water, contains 15-20% water). All chemicals were used without further purification.

***Preparation of $CuCO_3$****:* 0.185 g of $Cu(NO_3)_2{\cdot}3H_2O$ was dissolved into 6.0 mL of deionized (DI) water. 1.2 Eq. of 1.0 M $K_2CO_3$ was added dropwise under vigorous stirring in an ice bath. The precipitates were centrifuged with iced DI water three times and methanol one time and dried under vacuum at room temperature.

***Preparation of $CuBaCO_3$****:* 0.185 g of $Cu(NO_3)_2{\cdot}3H_2O$ and 0.02 g $Ba(NO_3)_2$ was dissolved into 6.0 mL of deionized (DI) water. 1.2 Eq. of 1.0 M $K_2CO_3$ (Alfa-Aesar, 99%) was added dropwise under vigorous stirring in an ice bath. The precipitates were centrifuged with iced DI water three times and methanol one time and dried under vacuum at room temperature.

***Preparation of CuBaCNT****:* Multi-walled carbon nanotubes (MWCNT) were added into 10% $HCl_{(aq)}$ under stirring overnight. After removing $HCl_{(aq)}$ by vacuum filtration, 0.5 g of MWCNT were sonicated in the solution of 75 mL $H_2SO_4$ and 25 mL $HNO_3$ for 6 hours and subsequently refluxed at 50 °C for 12 hours. The mixture was washed until reaching neutral and redispersed into 50 mL DI water (Ox-MWCNT) for further utilization.
0.185 g of $Cu(NO_3)_2{\cdot}3H_2O$, 0.02 g $Ba(NO_3)_2$, and 1 mL OX-MWCNT were added into 6.0 mL of deionized (DI) water. 1.2 Eq. of 1.0 M $K_2CO_3$ (Alfa-Aesar, 99%) was added dropwise under vigorous stirring in an ice bath. The precipitates were centrifuged with iced DI water three times and methanol one time and dried under vacuum at room temperature.

***Preparation of a gas-diffusion electrode by spray-coating****:* 2.3 mg of catalyst was mixed with 9 μL of Nafion solution (~5 wt%) and 225 μL of methanol. This dispersed ink was sprayed onto a PTFE substrate with an area loading of 1 mg $cm^{-2}$.

***Preparation of a sputtered Cu on PTFE substrate****:* Cu with a thickness of 300 nm was sputtered on a PTFE substrate (pore size of 450 nm) using a pure Cu target (99.99%) with an

Ar flow rate of 3 mtorr at a DC power of 30 Watts in a magnetron sputtering system. The base pressure is below 5 x $10^{-6}$ torr, acquired using a turbomolecular pump.

***Characterization:*** Microstructure was collected by field-emission scanning electron microscopy (FESEM, JEOL, JSM-6500F) equipped energy dispersive X-ray spectroscopy (EDX, Oxford Instrument INCAx-sight 7557). Cold-field emission Cs-corrected transmission electron microscope (JEOL ARM-200FTH) with 200 keV acceleration voltage was used in microstructure analysis at Department of Material Science and Engineering, National Tsing Hua University, Taiwan. The lattice fringes and elemental mapping of ex-situ measurements were collected with field-emission transmission electron microscopy (FE-TEM, JEOL-2100F) equipped energy dispersive X-ray spectroscopy (EDX, Oxford Instrument XMaxN TSR) at Department of Chemistry, National Taiwan University, Taiwan. The crystal structures were determined by synchrotron X-ray diffraction analysis (the incident X-ray wavelength of 0.7749 Å) at the BL01C2 beamline of TLS, NSRRC. X-ray photoelectron spectroscopy (XPS) measurements were conducted on an ULVAC-PHI PHI 5000 Versaprobe II photoelectron spectrometer at 2.4 × $10^{-10}$ torr using a monochromatic Al $K_\alpha$ X-ray beam (1486.60 eV). All binding energies (BEs) of the elements were calibrated to adventitious carbon at 284.6 eV. X-ray absorption spectroscopy (XAS) including X-ray absorption near edge spectra (XANES) and extended X-ray absorption fine structure (EXAFS) of Cu K-edge were collected in fluorescence mode using a Lytle detector at the BL17C beamline of TLS, BL44A beamline of TPS, and 12B2 beamline of SPring-8, NSRRC. The pre-edge baseline was subtracted and the spectra was normalized to the post-edge. EXAFS analysis was conducted using a Fourier transform on $k^2$-weighted EXAFS oscillations to evaluate the contribution of each bond pair to the Fourier transform peak. 1s3p Resonant inelastic X-ray scattering was collected by silicon drift detector (XR-100CR Si-PIN X-ray detector) in partial-fluorescence-yield mode, whose fluorescence was split by the analyzer crystal Si(111) facet, at the 12XU beamline of SPring-8, NSRRC. The Ba/Cu of the catalysts was quantified by inductively coupled plasma mass spectrometry (ICP-MS, Thermo Fisher Scientific iCAP TQ).

***Electrochemical measurement:*** Electrochemical properties were investigated using a Biologic VSP-3e potentiostat in a flow cell reactor using a gas diffusion electrode (GDE) as the working electrode (WE), nickel foam as the counter electrode (CE), and a saturated Ag/AgCl electrode as the reference electrode (RE). The WE and CE were separated by an anion exchange membrane. An aqueous solution of 1.0 M KOH was used as the electrolyte, and the flow rate

of $CO_2$ was 50 sccm. The potentials were converted to values relative to RHE based on the following equation: $E_{RHE} = E_{Ag/AgCl} + 0.0591 \times pH + E^0_{Ag/AgCl}$, where $E^0_{Ag/AgCl}$ is the standard potential of Ag/AgCl relative to SHE at 25 °C (0.210 V). The working area of electrodes was 1.0 $cm^2$ for each experiment. The gaseous products were evaluated via gas chromatography (Agilent 8860) equipped with a thermal conductivity detector and a flame ionization detector. $^1H$ NMR spectroscopy (400 MHz, Agilent 400-MRDD2 NMR spectrometer) with water suppression was used to analyze the liquid products using $D_2O$ and dimethylsulfoxide (DMSO) as the lock solvent and internal reference, respectively. We built the calibration curves via the ratio between $^1H$ peak in each liquid product and the DMSO peak to quantify the liquid products. The production of formate, acetic acid, and propanol is much lower than the detection limit of calibration, so we did not include these products in this study.

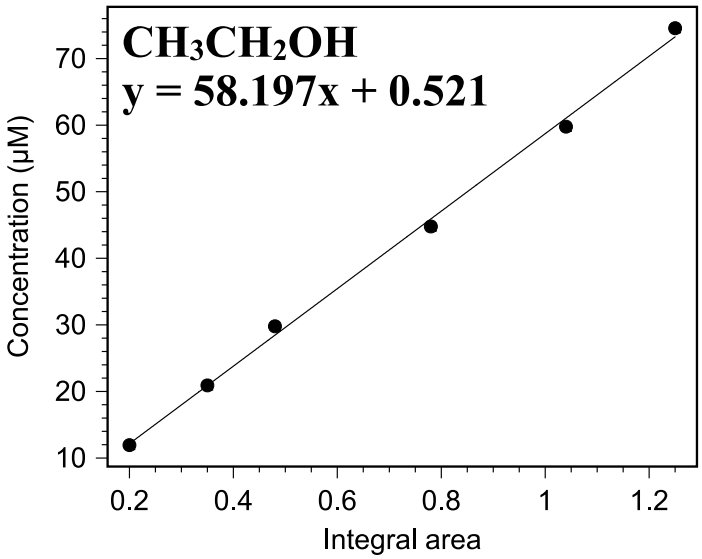


Calibration curve for ethanol using d-DMSO as the internal reference.

***Operando XAS measurement:*** *Operando* XAS was carried out in the same conditions as electrochemical testing using the designed flow cell with an opening sealed by Kapton tape in the gas chamber. The signal of X-ray absorption spectroscopy was collected in total-fluorescence-yield mode using a Lytle detector at the BL17C beamline of TLS, BL44A beamline of TPS, and 12B2 beamline of SPring-8, NSRRC.

***Operando Raman measurement:*** *Operando* Raman were conducted using a Renishaw inVia Raman microscope in a modified flow cell with a water immersion objective, employing a diode laser at 785 nm. $CO_2$ with a flow rate of 50 sccm flowed through the gas chamber. An Ag/AgCl (3 M KCl) electrode and a nickel foam were used as the reference and counter electrode,

respectively. Working electrode and counter electrode was separated by an anion exchange membrane.

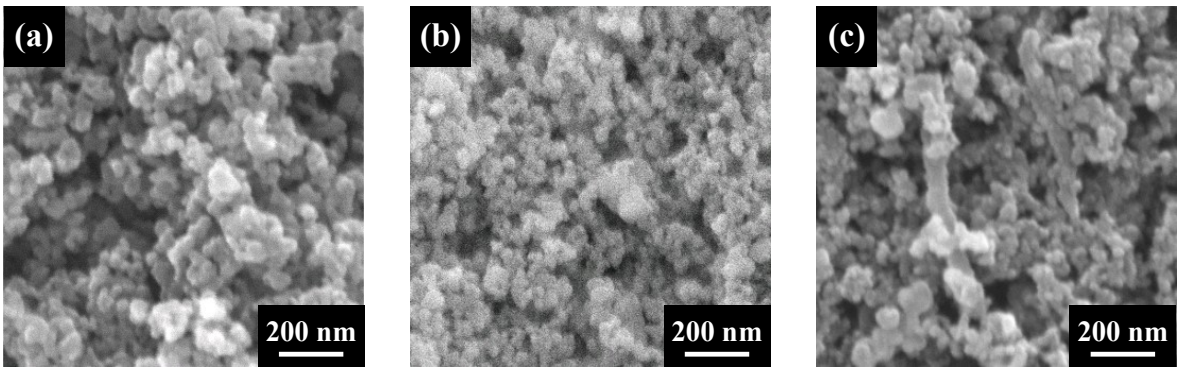


**Figure S1.** Scanning electron microscopic images of (a) $CuCO_3$, (b) $CuBaCO_3$, and (c) CuBaCNT.

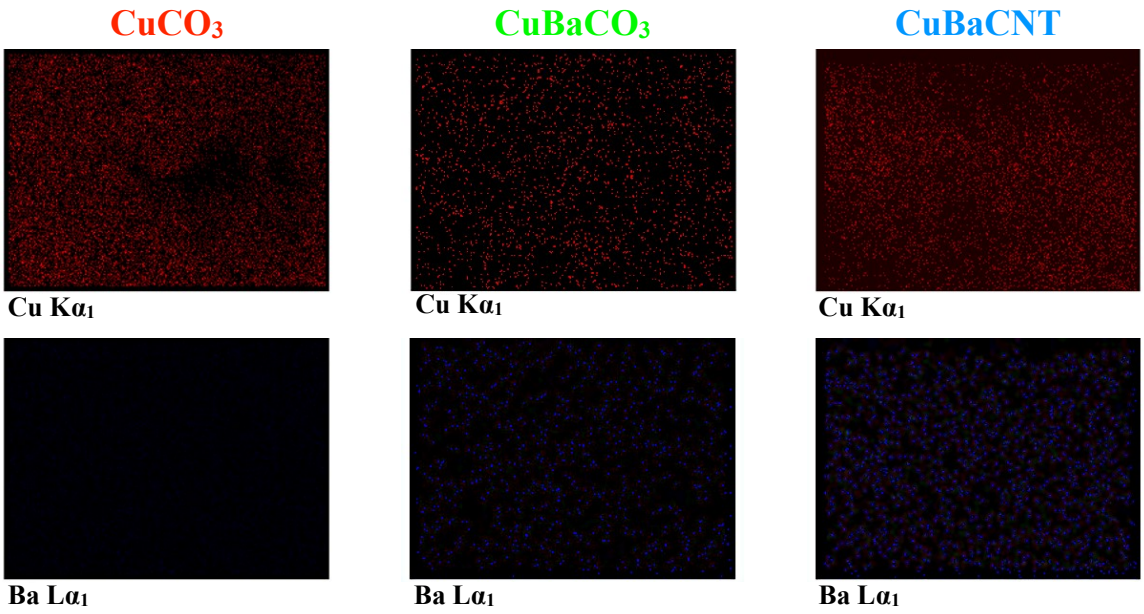


**Figure S2**. EDX mapping of Cu $K_{\alpha 1}$ and Ba $L_{\alpha 1}$ of $CuCO_3$, $CuBaCO_3$, and CuBaCNT.

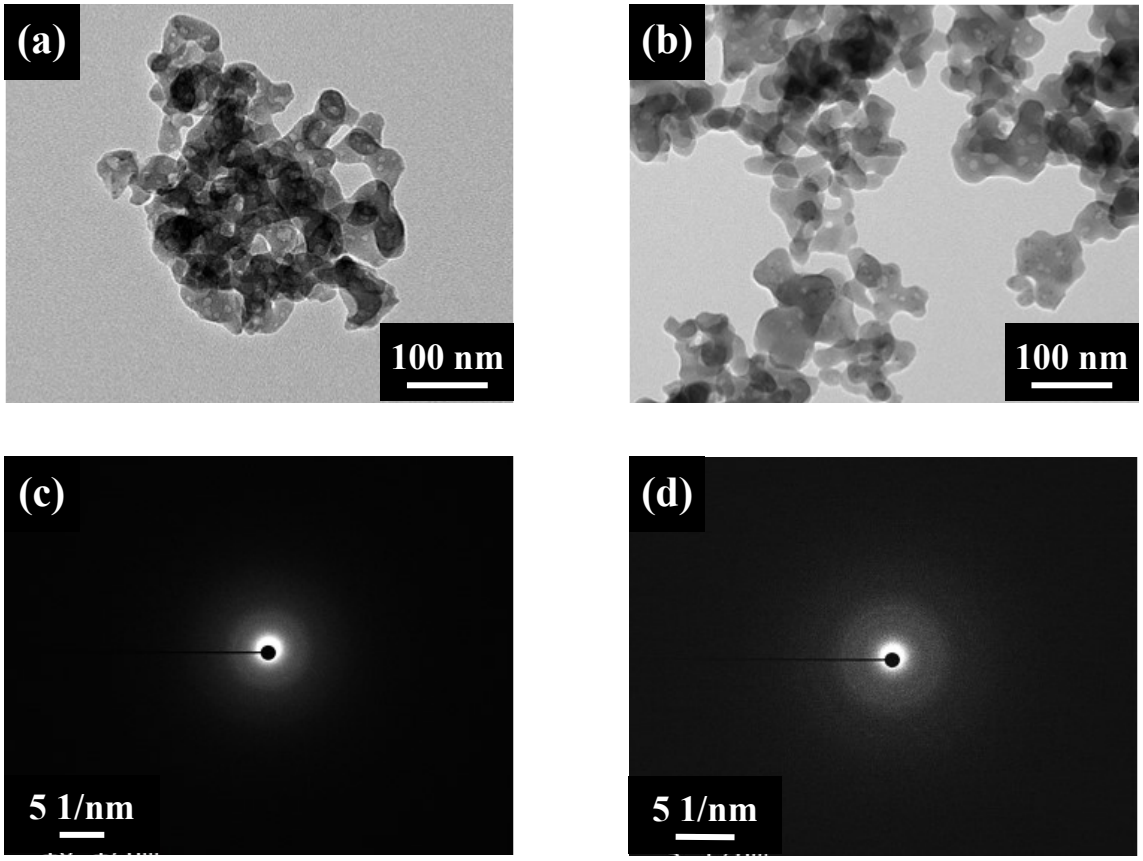


**Figure S3.** Transmission electron microscopic images of (a) $CuCO_3$ and (b) $CuBaCO_3$. Selected area electron diffraction patterns of (c) $CuCO_3$ and (d) $CuBaCO_3$.

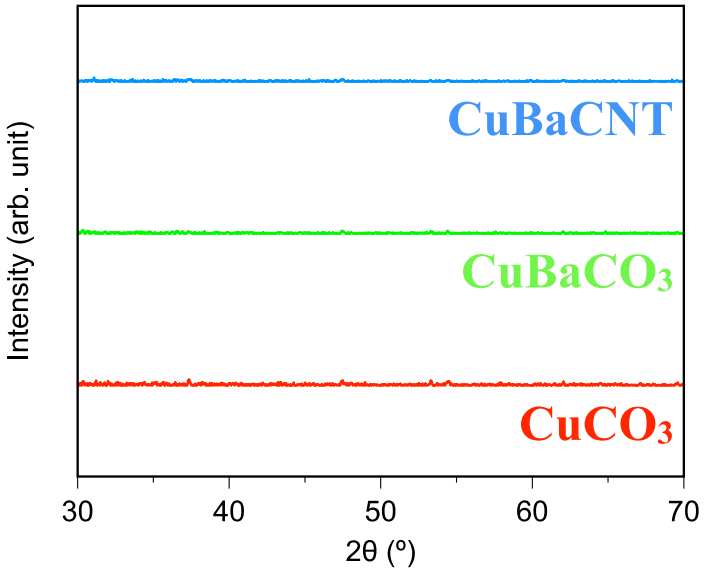


**Figure S4.** Synchrotron X-ray diffraction (SXRD) patterns of $CuCO_3$, $CuBaCO_3$, and CuBaCNT.

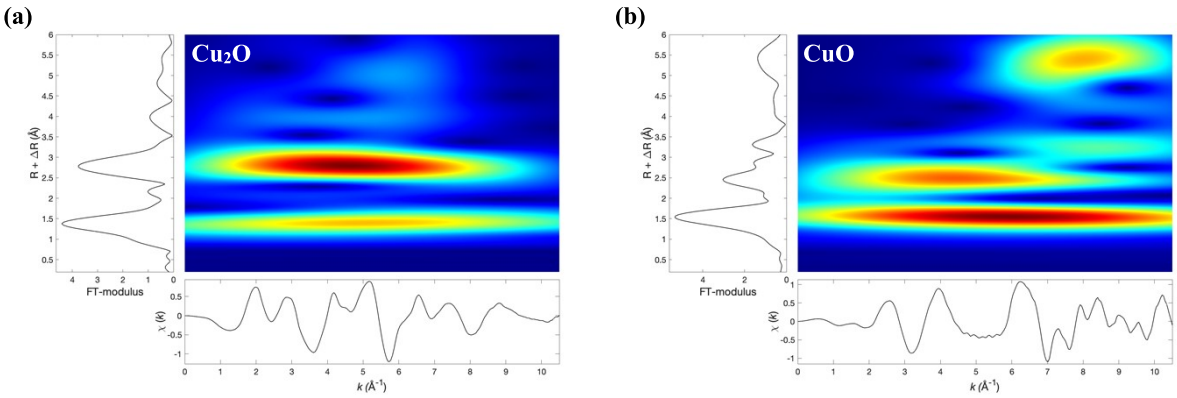


**Figure S5.** Wavelet analysis of $Cu_2O$ and CuO standards.

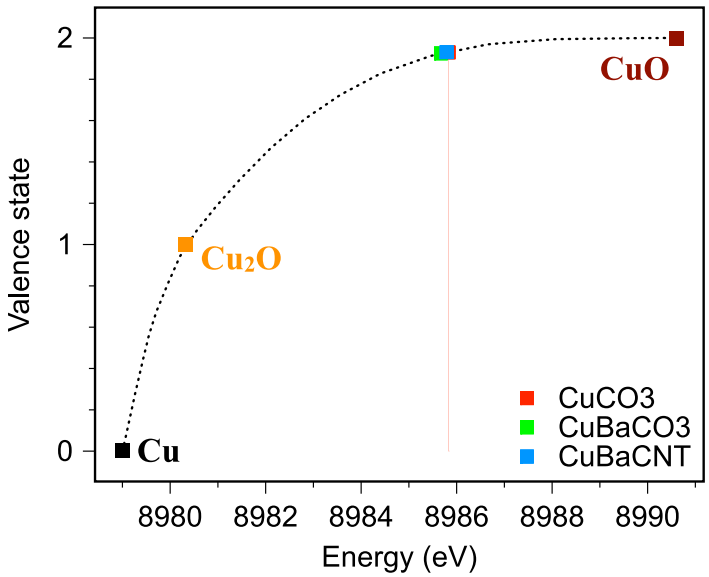


**Figure S6.** Valence-state analysis of $CuCO_3$, $CuBaCO_3$, and CuBaCNT. The corresponding valence states were obtained by the first-derivative of the XANES spectra using Cu foil, $Cu_2O$, and CuO as references.

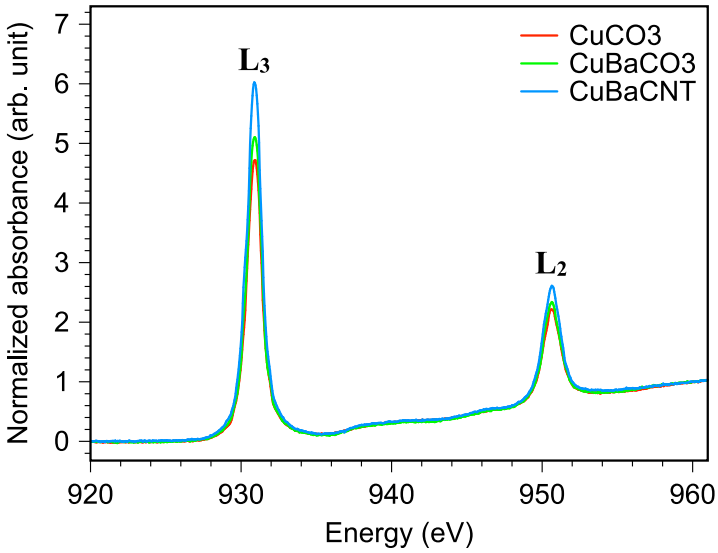


**Figure S7.** Cu L-edge XAS spectra of $CuCO_3$, $CuBaCO_3$, and CuBaCNT.

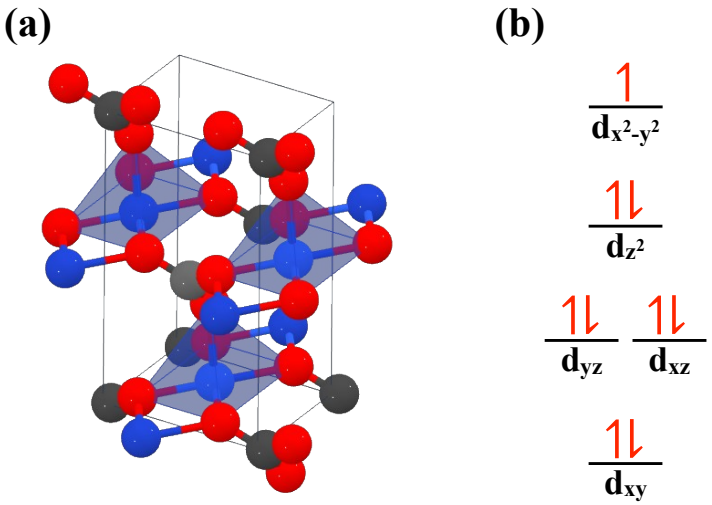


**Figure S8.** (a) Crystal structure of $CuCO_3$, obtained from Material Project. Blue, red, and black balls are copper, oxygen, and carbon, respectively. The coordination environment of copper is a distorted square pyramidal. (b) The corresponding d-orbital energy diagram.

Material Project Ref: Anubhav Jain, Shyue Ping Ong, Geoffroy Hautier, Wei Chen, William Davidson Richards, Stephen Dacek, Shreyas Cholia, Dan Gunter, David Skinner, Gerbrand Ceder, Kristin A. Persson; Commentary: The Materials Project: A materials genome approach to accelerating materials innovation. *APL Mater* 1 July 2013; 1 (1): 011002. https://doi.org/10.1063/1.4812323

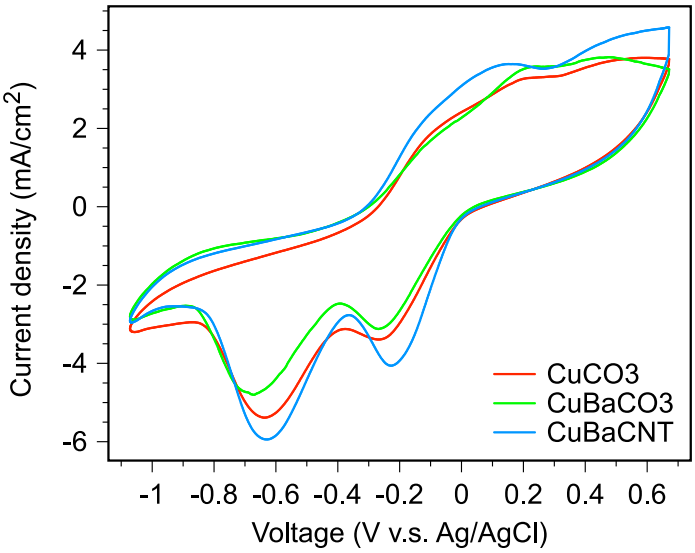


**Figure S9.** Cycling voltammetry curves of $CuCO_3$, $CuBaCO_3$, and CuBaCNT.

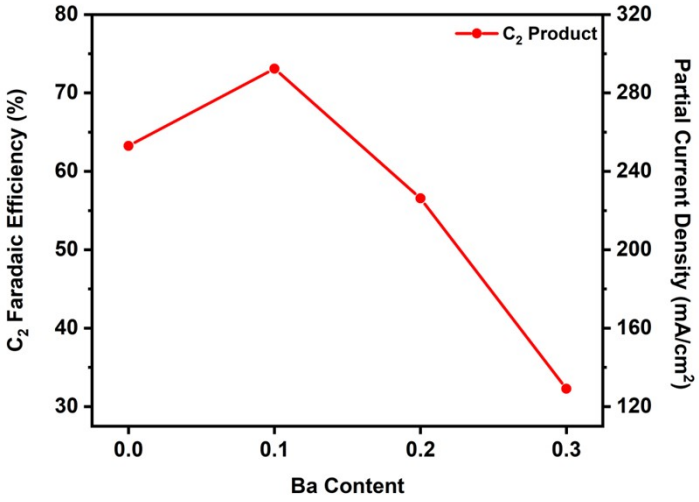


**Figure S10.** Catalytic activities of $CuBaCO_3$ at 400 mA/cm$^2$ with various Ba content.

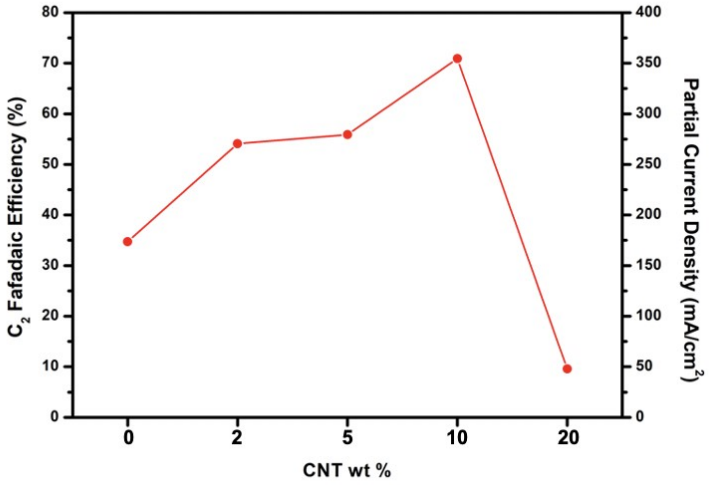


**Figure S11.** Catalytic activities of CuBaCNT at 500 mA/cm$^2$ with various CNT addition.

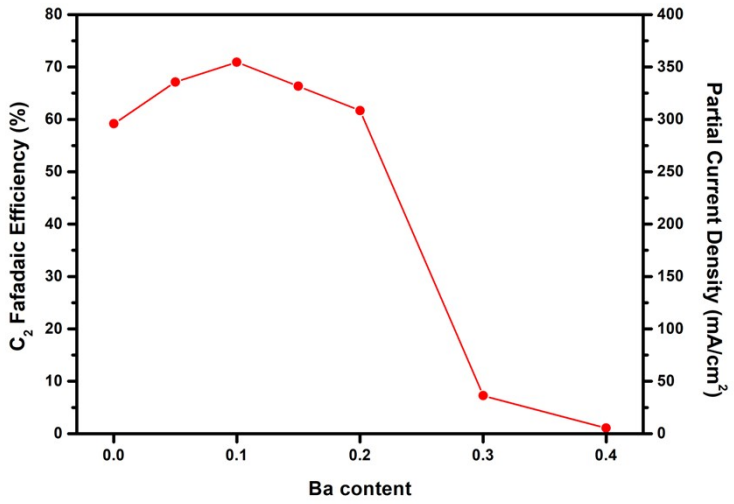


**Figure S12.** Catalytic activities of CuBaCNT at 500 mA/cm$^2$ with various Ba content. First, when barium ions are introduced into $CuCO_3$/CNT, the Faradaic efficiency and partial current density of C2 products increase and optimize at the barium content of 0.2 compared to the copper concentration, which we achieve 70.9% Faradaic efficiency and partial current density of 354.6 mA cm$^{-2}$ to C2 products at 500 mA cm$^{-2}$. We attribute this enhancement to an orbital interaction of barium ions to the copper sites. Then, when we further increase the amount of barium ions, the overall $CO_2$RR activity drops, and hydrogen evolution escalates. We reason that copper active sites are still in charge of the $CO_2$RR conversion, so the insufficient quantity deteriorates the activity. When the barium content increases to 0.4, the hydrogen evolution dominates. Thus, we believe the barium ions play a role in modifying copper active sites rather than exhibiting $CO_2$RR capability.

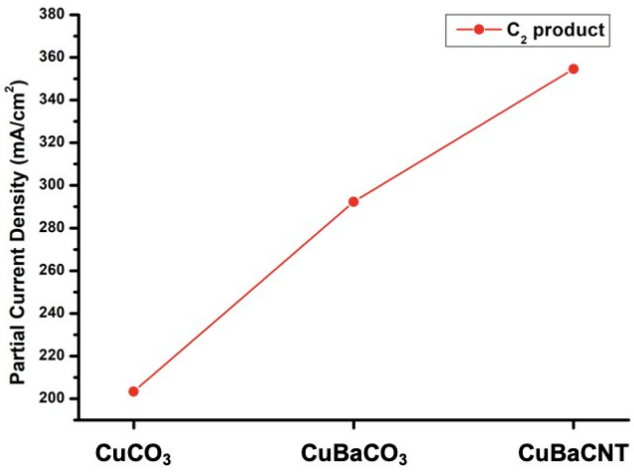


**Figure S13.** Partial current density to C2 products of $CuCO_3$, $CuBaCO_3$, and CuBaCNT at the highest Faradaic efficiency to C2 products.

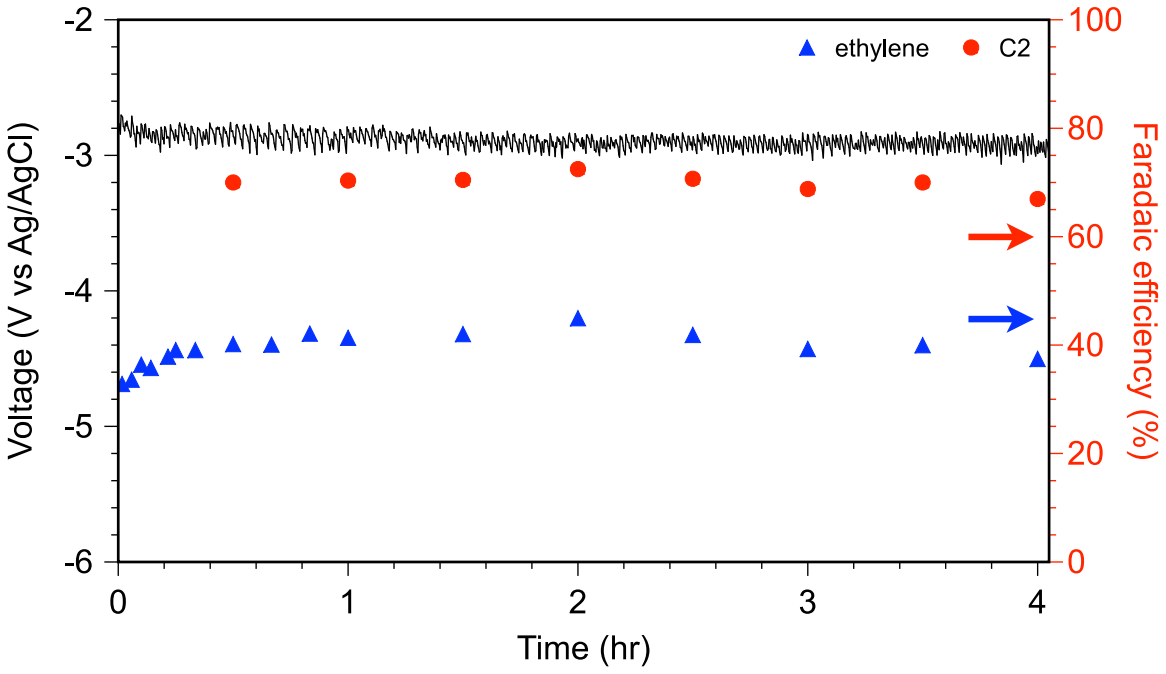


**Figure S14.** Catalytic stability of CuBaCNT toward ethylene and C2 products at 500 mA/cm$^2$.

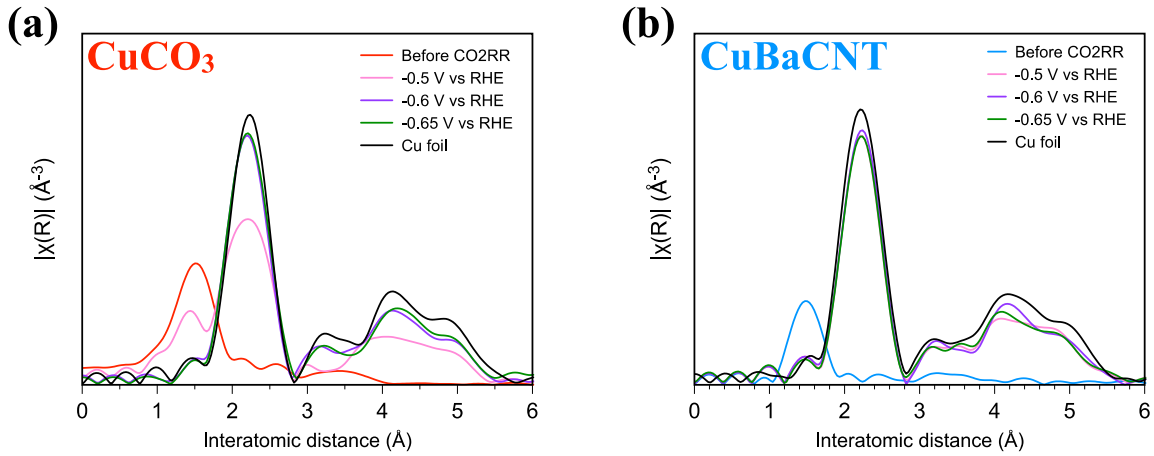


**Figure S15.** In-situ extended X-ray absorption fine structure (EXAFS) of Cu K-edge for (a) $CuCO_3$ and (b) CuBaCNT.

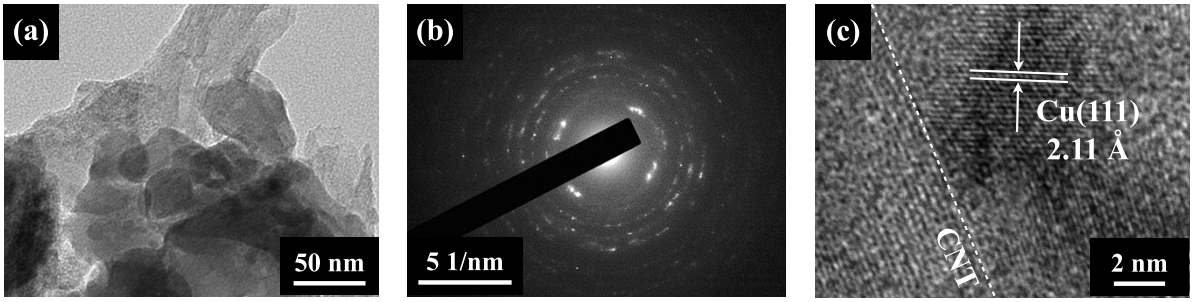


**Figure S16.** (a) Transmission electron microscopic image, (b) selected area electron diffraction pattern, and (c) high-resolution image of CuBaCNT after $CO_2$RR.

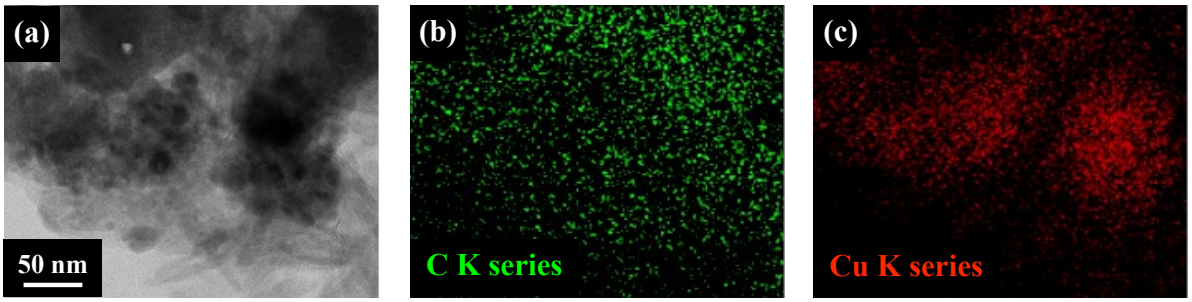


**Figure S17.** (a) Transmission electron microscopic image and the corresponding EDX mapping of (b) C K-series and (c) Cu K-series for CuBaCNT after $CO_2$RR.

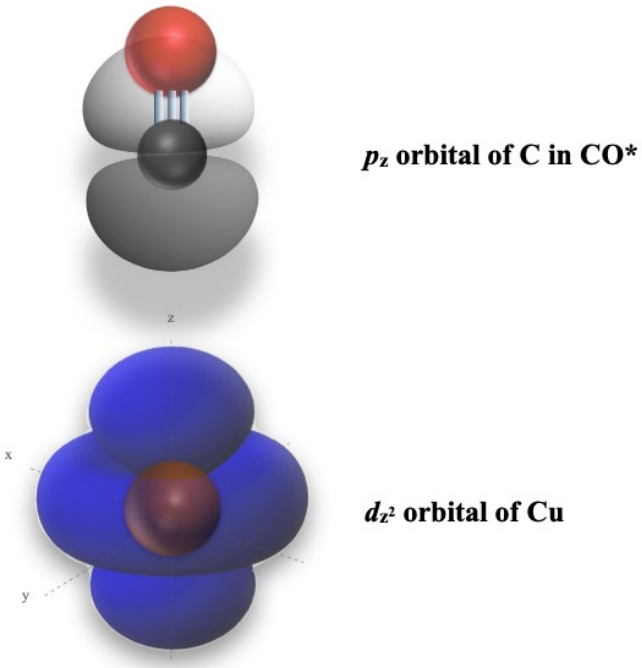


**Figure S18.** The interaction between the Cu $3d_{z^2}$ orbital with carbon $2p_z$ orbital of carbon in CO*.

**Table S1.** Comparison of electrochemical $CO_2$-to-C2 products (ethylene and ethanol) performance with total current density higher than 100 mA $cm^{-2}$.

| Catalyst | $FE_{C2}$ (%) | $J_{C2}$ (mA/$cm^2$) | $J_{total}$ (mA/$cm^2$) | Reference |
|---|---|---|---|---|
| **CuBaCNT** | **71** | **355** | **500** | **This work** |
| Cu(OH)BTA | 68 | 340 | 500 | *Nat. Commun,* 2023, 14, 474 |
| Cu/FeTPP[Cl] | 78 | 234 | 300 | *Nat. Catal.* 2020, 3, 75 |
| Cu(OH)x/Cu | 77 | 231 | 300 | *Nat. Commun,* 2019, 10, 5814 |
| $SrCuO_2$ | 53 | 106 | 200 | *ACS Catal.* 2022, 12, 6663 |
| Cutrz | 80 | 224 | 280 | *ACS Catal.* 2022, 12, 8444 |
| OD-Cu | 75 | 225 | 300 | *J. Am Chem. Soc.* 2022, 144, 259 |
| Cu-$CeO_2$ | 56 | 140 | 250 | *Adv. Mater.* 2023, 35, 2208996 |